A Data-Fusion Approach for Speed Estimation and Location Calibration of a Metro Train Based on Low-Cost Sensors in Smartphones

Yuan Wang, Jianli Cong, Ping Wang, Xiang Liu, and Huiyue Tang

***Abstract*— Since the GPS is unavailable in underground environment, it is extremely challenging to measure the speed and location of a metro train. This paper proposes a novel data-fusion approach for speed estimation and location calibration of a metro train in underground environment, simply using the data from the 3-axis accelerometers in smartphones. Firstly, we place multiple smartphones in different cars of a train to measure the longitudinal, lateral and vertical accelerations, then propose a method to transform the measured accelerations from the coordinate systems of smartphones to that of the metro train. In the data fusion model, the initial estimations of train speed and position are obtained by the integral and double integral of the longitudinal accelerations. The lateral and vertical accelerations are used to provide absolute reference for speed estimation, where the local time delay and waveform similarity between the measured accelerations in different smartphones are defined and estimated to obtain the time-delay-based speed. Finally, a more accurate estimation of train speed is obtained by fusing the integral-based speed and the time-delay-based speed. A case study is conducted on Chengdu Metro Line 7 in Chengdu, China. The results show that, taking the interval length between adjacent stations as ground truth, our data-fusion approach achieves higher accuracy than the direct integral method, with the relative errors reduced from 9.5% to 1.6%.**

***Index Terms*— Data fusion, speed estimation, location calibration, coordinate system transformation, metro train.**

Manuscript received June 9, 2019; revised July 31, 2019; accepted August 4, 2019. Date of publication August 7, 2019; date of current version October 17, 2019. This work was supported in part by the National Natural Science Foundation of China under Grant 51425804, Grant 51608459, and Grant 51378439 and in part by the United Fund for Key Projects of China's High-Speed Railway under Grant U1334203 and Grant U1234201. The work of Y. Wang and H. Tang was supported by the China Scholarship Council (CSC) under Grant 201707000036 and Grant 201707000037. The associate editor coordinating the review of this article and approving it for publication was Dr. Ashish Pandharipande. *(Corresponding author: Huiyue Tang.)*

Y. Wang is with the MOE Key Laboratory of High-speed Railway Engineering, Southwest Jiaotong University, Chengdu 610031, China, and also with the Department of Civil and Environmental Engineering, Rutgers, The State University of New Jersey, New Brunswick, NJ 08854 USA.

J. Cong and P. Wang are with the MOE Key Laboratory of High-speed Railway Engineering, Southwest Jiaotong University, Chengdu 610031, China.

X. Liu is with the Department of Civil and Environmental Engineering, Rutgers, The State University of New Jersey, New Brunswick, NJ 08854 USA.

H. Tang is with the School of Electrical Engineering, Southwest Jiaotong University, Chengdu 610031, China, and also with the Department of Civil and Environmental Engineering, Rutgers, The State University of New Jersey, New Brunswick, NJ 08854 USA (e-mail: huiyue@my.swjtu.edu.cn).

Digital Object Identifier 10.1109/JSEN.2019.2933638

I. Introduction

SPEED estimation and location calibration are very important for safe and efficient operation of trains, since i) the real-time measurement of speed and location can be used by the Automatic Train Control (ATC) system, to determine the change of traction/braking force [1]. ii) Speed-location curves can be used to analyze the train dynamics [2], which builds a foundation for finding the optimal train control strategies [3].

There are typically two approaches for improving the accuracy of speed estimation and train positioning: i) improving the measurement equipment with cutting-edge techniques and ii) developing new algorithms to fuse the measured data from different sources to achieve higher accuracy. Firstly, there are quite many techniques for speed and location measurement, such as Global Navigation Satellite System (GNSS) [4]–[10], Doppler radar [11], ultra-wideband radios [12], tachometers [13], [14] and various methods based on inertial measurement unit (IMU) sensors [4], [10], [15]–[17]. Secondly, a lot of data-fusion algorithms are developed to fuse different data sources. GNSS and IMU are the most commonly used data sources for train positioning [18]–[27]. Kalman Filter (KF) [28] and its variants, such as Extended Kalman Filter (EKF) [29], Unscented Kalman Filter (UKF) and Cubature Kalman Filter (CKF) [30], [31], are the most poupular algorithms for GNSS/INS integration. Furthermore, Particle Filter (PF) [32], [33] is also useful for GNSS/INS integration. There is a detailed review regarding those techniques and data-fusion algorithms [4]. In particular, using tachometers is an effective approach for speed estimation [14], and fusing the data from tachometers and IMU can further improve the results of speed and position estimation [13].

Map matching is a useful approach for train positioning. In [34], [35], the rail track curvatures are identified using low-cost IMU sensors, and the angular rate and the longtitudinal speed are measured by a yaw gyro and an odometer, respectively. Then Kalman filters are utilized to fuse the yaw rate and the tachometer signals. Similar approaches can be found in [36]–[38], where a precise digital map is used as an essential reference to relate the measured sensor data to track geometry. The benefit of map matching is that it introduces an absolute reference, which can be used to update the current position information and restrain the accumulation of positioning error.

Notably, a precise digital map is essential for using the map matching method.

Unfortunately, none of the existing approaches can satisfy our requirements. The difficulties and challenges are given as the following points:

i) Generally, metro trains run in underground environment, where the Global Positioning System (GPS) signals cannot be received, so the GNSS is not available. All the GNSS/INS integration algorithms cannot be used.
ii) Both Doppler radar and ultra-wideband radio techniques need systematic equipment, which are much more expensive and inconvenient than using smartphones.
iii) IMU sensor seems promising, but it suffers from inertial drift [39]. The integral of the measured acceleration over several kilometers may lead to a position error of several hundred meters.
iv) As for the map matching approach, the problem is that, for metro lines, the curved tracks generally locate near the stations. When the trains run across these curved tracks, the accelerations and decelerations can make the inertial signals unstable, which may result in large positioning errors.
v) Although trains are usually equipped with more accurate accelerometers and tachometers, which can provide accurate speed and location, all the information from those sensors are not accessible to other mobile devices because of security issues.

This paper aims to develop a novel data-fusion approach to estimate the speed and position of a metro train that runs in underground environment, simply using the data from the 3-axis accelerometers in smartphones. As illustrated in Fig. 1, instead of using one smartphone, we use multiple smartphones to measure the accelerations of different cars of a metro train. This paper is based on following considerations: i) the longitudinal (the running direction of the train) accelerations provide detailed but biased information of speed and location by integral and double integral, respectively. ii) The vertical (the opposite direction of gravity) accelerations, the lateral (the direction perpendicular to both the longitudinal direction and the vertical direction) accelerations, and the relative distance between smartphones can provide absolute reference for speed estimation. iii) The accuracy of speed estimation and location calibration can be improved by fusing the longitudinal, lateral and vertical accelerations from multiple smartphones.

The contributions of this paper are presented as follows.

i) This paper proposes a novel data-fusion approach for speed estimation and location calibration of a metro train in underground environment, simply using the data from the low-cost 3-axis accelerometers in smartphones, which can (1) be used when GPS signals are not available, (2) restrain the influence of inertial drift, and thus improve the accuracy of speed and position estimation. Taking the interval lengths between adjacent stations as ground truth, mostly, the estimation errors of our data-fusion approach are below 20 meters, where the mean value of the interval lengths between adjacent stations is 1310 meters, so the relative error is 1.6%. By contrast, the relative error of the direct integral method is 9.5%. Our data-fusion approach can be used to provide speed and location information for riding smoothness assessment and noise assessment of underground rail lines using mobile device.
ii) This paper proposes a method to transform the measured accelerations from the coordinate systems of smartphones to that of the metro train. With this method, it is no longer required to adjust the directions of the smartphones and fix them to specific positions during the measuring process. The measurement based on the 3-axis accelerometers of smartphones becomes much more convenient.

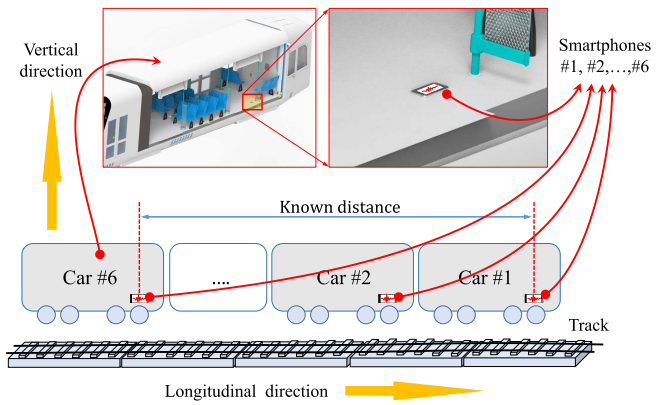

Fig. 1. Smartphones on a metro train, at least one smartphone in each car.

This paper is organized as follows. Section II introduces the tools and methods for data acquisition and preprocessing, where the measurement condition and the method for correcting the coordinate system are given. Section III introduces the data fusion approach for estimating the speed and location using the 3-axis accelerations measured by smartphones. Section IV uses a case study carried out on Chengdu Metro line 7 to demonstrate the data-fusion approach proposed in this paper. Section V discusses the factors that influence the performance of the data fusion approach. Section VI gives the conclusion.

II. Data Acquisition and Preprocessing

A. APP Design and Measurement Condition

We have designed an exclusive Android APP to record the acceleration of metro train. The sampling frequency is 100Hz. Data acquisition is conducted on an in-service metro train consisting of six cars. In each car, there is a smartphone placed (not fixed for the consideration of convenience) on the floor, and close to the front bogie. There are totally 28 stations on the metro line, so there are 27 intervals. It takes 1.14 hours for the train to travel from the first station to the last station, which is called one run. The data of three runs are recorded in our tests.

After data acquisition, it is necessary to do data preprocessing, including the following steps:

i) *Outliers elimination*. The thresholds for the absolute values of the longitudinal, lateral and vertical accelerations are all set to 1.5m/s^2.

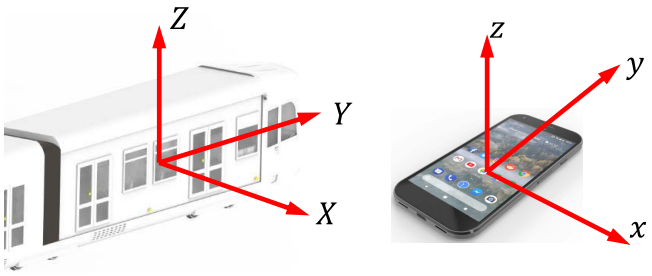

The coordinate system of a metro train

The coordinate system of a smartphone

Fig. 2. The coordinate systems of the metro train and the smartphone.

ii) *Signal resampling*. The sampling frequency of the raw data is 100Hz, but there is a little variance, so re-sampling is performed based on cubic spline interpolation.

iii) *Time synchronization*. Since the timestamps of different smartphones are different, we use the correlation function to estimate the time difference and then synchronize the data of all smartphones.

B. Coordinate System Transformation

The coordinate systems of a metro train and a smartphone are shown in Fig. 2, where X, Y and Z denote the lateral, longitudinal and vertical directions of the coordinate system of the metro train, respectively, and x, y and z denote the lateral, longitudinal and vertical directions of the coordinate system of the smartphone, respectively. Since the smartphone is simply placed on the floor of a car rather than fixed on it, the coordinate system of the smartphone may be different from that of the metro train. The measured accelerations are originally in the coordinate system of the smartphone. Since the measured accelerations are used to estimate the speed and position of the metro train, it is necessary to develop a method to transform the accelerations from the coordinate system of the smartphone to that of the metro train.

There are two principles for coordinate system transformation:

Principle 1: The vertical direction of the metro train is defined as the opposite direction of gravity;

Principle 2: The longitudinal and lateral accelerations of the metro train are independent and unrelated.

Coordinate system transformation includes two steps:

1) the transformation of the vertical direction;

2) the transformation of the longitudinal and lateral directions.

1) The Transformation of the Vertical Direction: Fig. 3(a) shows the transformation of the vertical direction. The color orange (X-Y-Z) represents the coordinate system of the metro train, the color blue (x-y-z) represents the coordinate system of the smartphone.

According to **Principle 1**, the vertical direction of the metro train (the direction of the Z axis) is the opposite direction of gravity. Considering that the tracks in metro stations are nearly horizontal, when a train stops at a station, the accelerations along the X axis and Y axis of a metro train are both zeros, only the accelerations along the Z-axis are non-zero values due

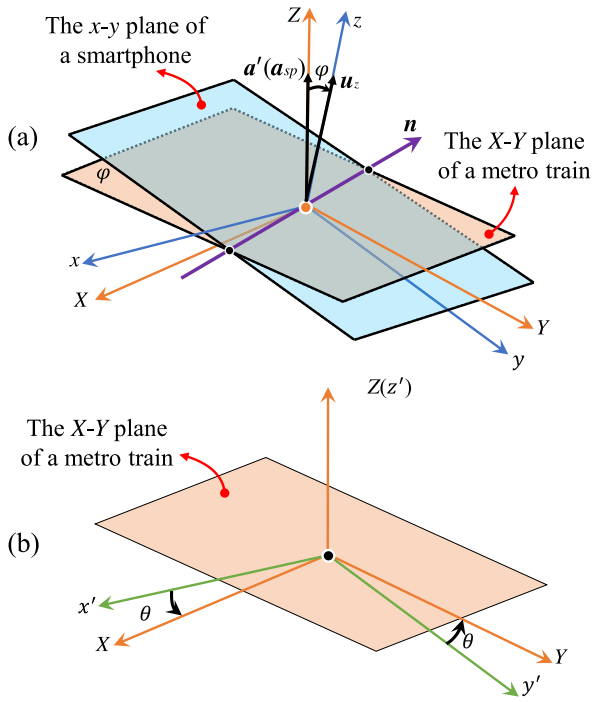

Fig. 3. The coordinate system transformation. (a) shows the transformation of the vertical direction, and (b) shows the transformation of the longitudinal and lateral directions. Color orange (X-Y-Z) represents the coordinate system of the metro train, color blue (x-y-z) represents the coordinate system of the smartphone, and color green (x'-y'-z') represents the coordinate system just after the transformation of the vertical direction.

to gravity. Therefore, only the accelerations measured when the train stops at a station are used for the transformation of the vertical direction.

Let $\boldsymbol{a}_{sp} = [a_x\ a_y\ a_z]^T$ denote the 3-axis accelerations output by a smartphone, and $\boldsymbol{a}' = [a_{x'}\ a_{y'}\ a_{z'}]^T$ denote the accelerations after the transformation of the vertical direction. Define the unit vector along the vertical direction Z is $\boldsymbol{a}' = [0\ 0\ 1]^T$. When $\boldsymbol{a}'$ is measured by a smartphone, the output of the smarphone is $\boldsymbol{a}_{sp}$.

The transformation of the vertical direction can be achieved by finding a matrix $\boldsymbol{R}$ satisfying

$$\boldsymbol{a}' = \boldsymbol{R}\boldsymbol{a}_{sp} \tag{1}$$

The mapping in (1) is equivalent to rotate $\boldsymbol{a}_{sp}$ to the direction of the z axis in the coordinate system of the smartphone. Denote $\boldsymbol{u}_z = [0\ 0\ 1]^T$ as the unit vector along the z axis in the coordinate system of the smartphone. The matrix $\boldsymbol{R}$ also satisfies (2).

$$\boldsymbol{u}_z = \boldsymbol{R}\boldsymbol{a}_{sp} \tag{2}$$

According to the Rodrigues' rotation formula, matrix $\boldsymbol{R}$ can be obtained by

$$\boldsymbol{R}(\boldsymbol{n}, \varphi) = \boldsymbol{I}\cos\varphi + (\sin\varphi)\boldsymbol{K} + (1-\cos\varphi)\boldsymbol{n}\boldsymbol{n}^T \tag{3}$$

where, $\boldsymbol{I}$ is the identity matrix. $\boldsymbol{n} = [n_x\ n_y\ n_z]^T$ is the rotation axis, which is perpendicular to both $\boldsymbol{u}_z$ and $\boldsymbol{a}_{sp}$, as defined in (4).

$$\boldsymbol{n} = \frac{\boldsymbol{a}_{sp} \times \boldsymbol{u}_z}{|\boldsymbol{a}_{sp} \times \boldsymbol{u}_z|} = \left[\frac{a_y}{\sqrt{a_x^2 + a_y^2}}\ \frac{-a_x}{\sqrt{a_x^2 + a_y^2}}\ 0\right]^T \tag{4}$$

where, $\boldsymbol{a}_{sp} \times \boldsymbol{u}_z$ is the cross product of $\boldsymbol{a}_{sp}$ and $\boldsymbol{u}_z$. $\left|\boldsymbol{a}_{sp} \times \boldsymbol{u}_z\right|$ is the magnitude of $\boldsymbol{a}_{sp} \times \boldsymbol{u}_z$.

Matrix $\boldsymbol{K}$ is determined by $\boldsymbol{n}$, as defined in (5).

$$\boldsymbol{K} = \begin{bmatrix} 0 & -n_z & n_y \\ n_z & 0 & -n_x \\ -n_y & n_x & 0 \end{bmatrix} \tag{5}$$

φ is the angle between $\boldsymbol{u}_z$ and $\boldsymbol{a}_{sp}$, as defined in (6).

$$\varphi = \arccos\left(\frac{\boldsymbol{a}_{sp} \cdot \boldsymbol{u}_z}{|\boldsymbol{a}_{sp}|\,|\boldsymbol{u}_z|}\right) \tag{6}$$

where, $\boldsymbol{a}_{sp} \cdot \boldsymbol{u}_z$ is the dot product of $\boldsymbol{a}_{sp}$ and $\boldsymbol{u}_z$. $\left|\boldsymbol{a}_{sp}\right|$ and $|\boldsymbol{u}_z|$ are the magnitudes of $\boldsymbol{a}_{sp}$ and $\boldsymbol{u}_z$, respectively.

2) The Transformation of the Longitudinal and Lateral Directions: The transformation of the longitudinal and lateral directions is performed after the transformation of the vertical direction. As shown in Fig. 3(b), by the transformation of the vertical direction, new coordinate system x'-y'-z' is obtained, which is plotted in green. The directions of Z axis and z' axis are the same, and the plane X-Y are the same with plane x'-y'. However, there is an angle θ between X axis and x' axis. Besides, θ is also the angle between Y axis and y' axis.

The transformation of the longitudinal and lateral direction can be achieved by estimating the angle θ.

Let $\boldsymbol{a}_{tr} = [a_X\ a_Y\ a_Z]^T$ denote the accelerations after the transformation of the longitudinal and lateral directions. Notably, $\boldsymbol{a}_{tr}$ are also the accelerations in the coordinate system of the metro train.

Consider the x'-y' plane, if the $[a_{x'}\ a_{y'}]^T$ rotates clockwise by angle θ, the rotated vector $[a_X\ a_Y]^T$ can be calculated by (7).

$$\begin{bmatrix} a_X \\ a_Y \end{bmatrix} = \begin{bmatrix} \cos\theta & \sin\theta \\ -\sin\theta & \cos\theta \end{bmatrix} \begin{bmatrix} a_{x'} \\ a_{y'} \end{bmatrix} \tag{7}$$

Since the directions of Z axis and z' axis are the same after the transformation of the vertical direction, we have $a_Z = a_{z'}$. Define $\boldsymbol{u}_Z = [0\ 0\ 1]^T$ as the unit vector along the Z axis in the coordinate system of the metro train, and $\boldsymbol{R}(\boldsymbol{u}_Z, \theta)$ as the matrix for the transformation of the longitudinal and lateral directions, we get

$$\boldsymbol{a}_{tr} = \boldsymbol{R}(\boldsymbol{u}_Z, \theta)\boldsymbol{a}' \tag{8}$$

where,

$$\boldsymbol{R}(\boldsymbol{u}_Z, \theta) = \begin{bmatrix} \cos\theta & \sin\theta & 0 \\ -\sin\theta & \cos\theta & 0 \\ 0 & 0 & 1 \end{bmatrix} \tag{9}$$

According to **Principle 2**, the longitudinal and lateral accelerations of the metro train are independent and unrelated. Thus the angle θ can be estimated by minimizing the absolute value of the covariance between a_X and a_Y.

Let θ^* be the optimal estimated value of θ, we have

$$\theta^* = \arg\min_{\theta} \left|E\left((a_X - E(a_X))(a_Y - E(a_Y))\right)\right| \tag{10}$$

Considering $E\left(a_{x'}\right) = 0$ and $E\left(a_{y'}\right) = 0$, we get

$$E\left(a_X\right) = 0, \quad E\left(a_Y\right) = 0 \tag{11}$$

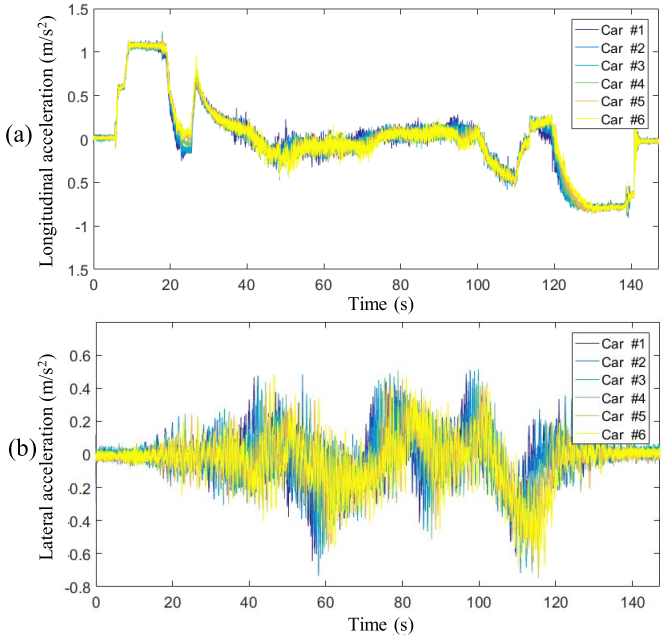

Fig. 4. The measured waveforms of the longitudinal and lateral accelerations (Interval 14 of Run 1).

Combining (7) and (11), we obtain that

$$\begin{aligned} &E\left((a_X - E(a_X))(a_Y - E(a_Y))\right) = E(a_X a_Y) \\ &= E\left((-a_{x'}^2 + a_{y'}^2)\sin\theta\cos\theta + a_{x'}a_{y'}(\cos^2\theta - \sin^2\theta)\right) \\ &= E(-a_{x'}^2 + a_{y'}^2)\sin\theta\cos\theta + E(a_{x'}a_{y'})(\cos^2\theta - \sin^2\theta) \\ &= \frac{1}{2}E(-a_{x'}^2 + a_{y'}^2)\sin 2\theta + E(a_{x'}a_{y'})\cos 2\theta \\ &= A\sin(2\theta + \gamma) \end{aligned} \tag{12}$$

where,

$$A = \sqrt{\frac{1}{4}E\left(-a_{x'}^2 + a_{y'}^2\right)^2 + E\left(a_{x'}a_{y'}\right)^2} \tag{13}$$

Therefore, we can get θ^* by

$$\theta^* = \frac{k\pi}{2} - \frac{1}{2}\arctan\left(\frac{2E(a_{x'}a_{y'})}{E(-a_{x'}^2 + a_{y'}^2)}\right), \quad k \in \mathbb{Z} \tag{14}$$

Finally, employing (1), (3), (8), (9) and (14), we obtain that

$$\boldsymbol{a}_{tr} = \boldsymbol{R}(\boldsymbol{u}_Z, \theta^*)\boldsymbol{R}(\boldsymbol{n}, \varphi)\boldsymbol{a}_{sp} \tag{15}$$

where, $\boldsymbol{a}_{tr}$ are the 3-axis accelerations in the coordinate system of the metro train, and $\boldsymbol{a}_{sp}$ are the 3-axis accelerations in the coordinate system of the smartphone.

After the data preprocessing, a sample of the measured longitudinal and lateral accelerations is presented in Fig. 4. It can be found that there is no delay between the longitudinal accelerations measured by different smartphones. In contrast, the lateral accelerations show obvious time delays as the car number increases. Notably, in addition to the integral of the longitudinal accelerations, the time delays of the lateral and vertical accelerations provide another way to estimate the running speed of the metro train. The next section will present a model to fuse all the available data to improve the precision of speed and location estimation.

III. Speed Estimation and Data Fusion

A. Direct Integral Method

Let $v(t)$ and $p(t)$ denote the speed and position of the metro train. When the speed $v(T)$ and the longitudinal acceleration $a_Y(\tau)$, $\tau \in [T, t)$ are known, the speed $v(t)$ can be estimated by direct integral, as shown in (16).

$$v(t) = v(T) + \int_T^t a_Y(\tau) d\tau \tag{16}$$

When the position $p(T)$, the speed $v(T)$ and the longitudinal acceleration $a_Y(\tau)$, $\tau \in [T, \tau_1]$ are available, the position $p(t)$ can be estimated by,

$$\begin{aligned} p(t) &= p(T) + \int_T^t v(\tau_1) d\tau_1 \\ &= p(T) + (t - T)v(T) + \int_T^t \int_T^{\tau_1} a_Y(\tau) d\tau d\tau_1 \end{aligned} \tag{17}$$

It is worth noting that the estimation of speed and position only based on the integral methods shown by (16)-(17) will lead to error accumulation as time increases, which is known as inertial drift phenomenon [39].

B. Data Fusion Approach

In the data-fusion model, the lateral and vertical accelerations are used to provide additional speed reference, therefore the accumulated error caused by the direct integral method can be restrained.

There are two basic assumptions:

i) The coupler stiffness of the metro train is large enough that the speed difference between the cars can be ignored;
ii) The relative distance between any two smartphones keeps constant.

The data fusion approach contains three parts:

i) *Time delay estimation*: This part estimates the time delays between the lateral or vertical accelerations from different smartphones.
ii) *Time-delay-based speed estimation*: This part obtains the time-delay-based speed points based on the estimated time delays and the relative distances between smartphones. The time-delay-based speed points are used to find the optimal estimated speed.
iii) *Speed correction*: This part introduces a method to correct the integral-based speed based on the optimal estimated speed.

Notably, only the vertical acceleration a_Z and the lateral acceleration a_X are used in i) Time delay estimation and ii) Time-delay-based speed estimation. To make the following deduction clear and concise, a is used to denote a_Z or a_X in i) and ii), and the results can be applied to both the vertical and lateral accelerations.

1) Time Delay Estimation: Firstly, the acceleration signals from Smartphones #i and #j are denoted by

$$\begin{aligned} \boldsymbol{a}_i &= \{a_i(0),\ a_i(\Delta t),\ a_i(2\Delta t),\ \ldots,\ a_i(N\Delta t)\} \\ \boldsymbol{a}_j &= \{a_j(0),\ a_j(\Delta t),\ a_j(2\Delta t),\ \ldots, a_j(N\Delta t)\} \end{aligned} \tag{18}$$

We define the local time delay $\delta(\boldsymbol{a}_i, \boldsymbol{a}_j)$ and the local waveform similarity $\rho(\boldsymbol{a}_i, \boldsymbol{a}_j)$ at time T as

$$\begin{cases} \delta(\boldsymbol{a}_i, \boldsymbol{a}_j) \triangleq \arg\max_{-\Lambda \le \varepsilon \le \Lambda} \mathbf{Cov}\left(\boldsymbol{a}_i(s, T), \boldsymbol{a}_j(s, T + \varepsilon)\right) \\ \rho(\boldsymbol{a}_i, \boldsymbol{a}_j) \triangleq \mathbf{Corr}\left(\boldsymbol{a}_i(s, T), \boldsymbol{a}_j(s, T + \delta(\boldsymbol{a}_i, \boldsymbol{a}_j))\right) \end{cases} \tag{19}$$

where, $\mathbf{Cov}(\cdot)$ and $\mathbf{Corr}(\cdot)$ are the operators for covariance and correlation coefficient, respectively. s denotes the matching length. $\boldsymbol{a}_i(s, T)$ and $\boldsymbol{a}_j(s, T)$ are sequences with central time T and length s, defined as

$$\begin{aligned} \boldsymbol{a}_i(s, T) = \Big\{ & a_i(T - (\tfrac{s}{2} - 1)\Delta t),\ a_i(T - (\tfrac{s}{2} - 2)\Delta t), \\ & \ldots,\ a_i(T + (\tfrac{s}{2} - 1)\Delta t),\ a_i\big(T + \tfrac{s}{2}\Delta t\big) \Big\} \end{aligned} \tag{20}$$

$$\begin{aligned} \boldsymbol{a}_j(s, T) = \Big\{ & a_j(T - (\tfrac{s}{2} - 1)\Delta t), a_j(T - (\tfrac{s}{2} - 2)\Delta t), \\ & \ldots,\ a_j(T + (\tfrac{s}{2} - 1)\Delta t),\ a_j\big(T + \tfrac{s}{2}\Delta t\big) \Big\} \end{aligned} \tag{21}$$

It can be interpreted that the local time delay $\delta(\boldsymbol{a}_i, \boldsymbol{a}_j)$ is defined as the local time shift ε that maximizes the covariance between $\boldsymbol{a}_i(s, T)$ and $\boldsymbol{a}_j(s, T + \varepsilon)$. The local waveform similarity $\rho_{i,j}$ is defined as the normalized correlation coefficient between $\boldsymbol{a}_i(s, T)$ and $\boldsymbol{a}_j(s, T + \delta(\boldsymbol{a}_i, \boldsymbol{a}_j))$.

To simplify the notation, we define

$$\delta_{i,j} = \delta(\boldsymbol{a}_i, \boldsymbol{a}_j), \quad \rho_{i,j} = \rho(\boldsymbol{a}_i, \boldsymbol{a}_j) \tag{22}$$

Furthermore, for $t < 0$ or $t > N\Delta t$, we specify $a_i(t) = 0$, $a_j(t) = 0$.

The definitions of the local time delay and the local waveform similarity have been introduced in our previous work for position sychronization of historical track inspection data [40]. Note that $\delta_{i,j}$ may not be equal to $\delta_{j,i}$ according to the definition in (19). We do not use the correlation function to estimate the time delay because the local waveform similarity $\rho_{i,j}$ may be biased when the local time delay $\delta_{i,j}$ is large and the matching length s is small.

The local time delays between the accelerations of different smartphones are caused by the relative distance between the smartphones and some significant features of track, such as track geometry irregularities due to turnouts, curvatures and ramps. As illustrated in Fig. 5, Car #i runs across a rail defect that can cause a large waveform, which is recorded by Smartphone #i. After a time interval $\delta_{i,j}$, Car #j runs across the same position and encounters a similar large waveform, which is recorded by Smartphone #j. Since $\delta_{i,j}$ can be estimated by (19), and the relative distance between the Smartphones #i and #j is known, the train speed at time T can be estimated.

2) Time-Delay-Based Speed Estimation: We establish a model to describe the mathematical relation between the relative distance between smartphones and the local time delay $\delta_{i,j}$.

Based on (19)-(22), we can obtain the local time delay $\delta_{i,j}$ and the local waveform similarity $\rho_{i,j}$. Let $v_{i,j}(t)$ denote the

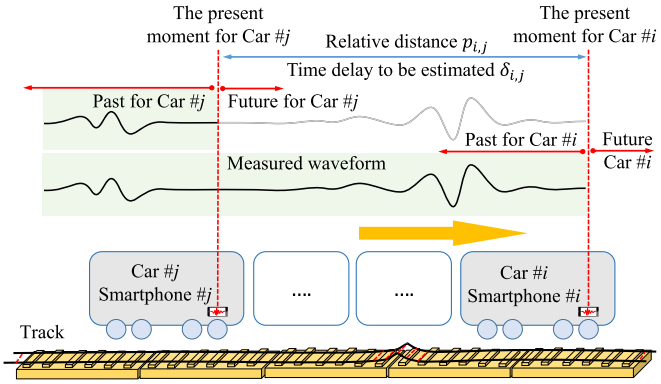

Fig. 5. The time delay of the lateral or vertical accelerations.

train speed between T and $T+\delta_{i,j}$, and $p_{i,j}$ denote the relative distance between Smartphones #i and #j, the relation between $p_{i,j}$ and $v_{i,j}(t)$ is shown in (23).

$$p_{i,j} = \int_{T}^{T+\delta_{i,j}} v_{i,j}(t)dt \tag{23}$$

Let $a_{Y,i}(t)$ be the longitudinal acceleration of Smartphone #i. $v_{i,j}(t)$ can be estimated by using (24).

$$v_{i,j}(t) = v_{i,j}(T) + \int_{T}^{t} a_{Y,i}(\tau)d\tau \tag{24}$$

Employing (23) and (24), we can obtain that

$$p_{i,j} = v_{i,j}(T)\delta_{i,j} + \int_{T}^{T+\delta_{i,j}} \int_{T}^{t} a_{Y,i}(\tau)d\tau dt \tag{25}$$

Therefore, $v_{i,j}(T)$ can be obtained by

$$v_{i,j}(T) = \frac{1}{\delta_{i,j}} \left(p_{i,j} - \int_{T}^{T+\delta_{i,j}} \int_{T}^{t} a_{Y,i}(\tau)d\tau dt \right) \tag{26}$$

where, $v_{i,j}(T)$ is called time-delay-based speed, since it is estimated based on the time delay between the accelerations from Smartphones #i and #j.

For each $\delta_{i,j}$ ($i \neq j$), there is a $v_{i,j}(T)$, hence a vector $\boldsymbol{v}$ can be constructed as follows.

$$\boldsymbol{v} = \left[\boldsymbol{v}_1^T \ \boldsymbol{v}_2^T \ \ldots \ \boldsymbol{v}_n^T \right]^T \tag{27}$$

where, $\boldsymbol{v}_i$ is

$$\boldsymbol{v}_i = \left[v_{i,1} \ \ldots \ v_{i,i-1} \ 0 \ v_{i,i+1} \ \ldots \ v_{i,n} \right]^T \tag{28}$$

where $v_{i,j} = v_{i,j}(T)$. Note that $v_{i,j}(T)$ is meaningless when $i = j$, so the value of $v_{i,i}(T)$ is set to zero.

It can be found that, in vector $\boldsymbol{v}$, there are $n(n-1)$ time-delay-based speed points for time T. However, according to the basic assumption, the speed difference between cars can be ignored, so the train speed at time T is unique. To obtain the optimal estimated speed $v^*(T)$, we propose the following optimization model.

$$\min_{v^*(T)} \frac{1}{2} (\boldsymbol{v}^*(T) - \boldsymbol{v})^T \operatorname{diag}(\boldsymbol{w}) (\boldsymbol{v}^*(T) - \boldsymbol{v}) \tag{29}$$

where, $\boldsymbol{v}^*(T)$ is a $n(n-1) \times 1$ vector that all the elements are $v^*(T)$. diag$(\cdot)$ is an operator for generating a diagonal matrix based on a given vector. $\boldsymbol{w}$ is the weight vector for balancing the uncertainties of $v_{i,j}(T)$. As shown in (30) and (31), $\boldsymbol{w}$ depends on the local waveform similarity $\rho_{i,j}$.

$$\boldsymbol{w} = \left[\boldsymbol{w}_1^T \ \boldsymbol{w}_2^T \ \ldots \ \boldsymbol{w}_n^T \right]^T \tag{30}$$

where, $\boldsymbol{w}_i = \left[w_{i,1} \ w_{i,2} \ \ldots \ w_{i,n} \right]^T$, with

$$w_{i,j} \begin{cases} 0, & i = j \text{ or } \rho < \rho_0 \\ \rho_{i,j}, & \text{otherwise} \end{cases} \tag{31}$$

where, ρ_0 is a threshold for filtering out the unreliable waveform matching pair.

Finally, the optimal estimated speed $v^*(T)$ can be obtained by

$$v^*(T) = \frac{1}{\|\boldsymbol{w}\|} \boldsymbol{w}^T \boldsymbol{v} \tag{32}$$

3) Speed Correction: Here the integral-based speed is corrected using the optimal estimated speed.

Firstly, let $\boldsymbol{v}_{\text{int}}$ denote the integral-based speed sequence,

$$\boldsymbol{v}_{\text{int}} = \{v_{\text{int}}(0), \ v_{\text{int}}(\Delta t), \ v_{\text{int}}(2\Delta t), \ \ldots, \ v_{\text{int}}(N\Delta t)\} \tag{33}$$

where, Δt is the sampling interval, in this paper $\Delta t = 0.01$s.

Then, let $\boldsymbol{v}_{\text{td}}$ denote the time-delay-based speed sequence,

$$\boldsymbol{v}_{\text{td}} = \{v_{\text{td}}(T_0), \ v_{\text{td}}(T_1), \ \ldots, \ v_{\text{td}}(T_M)\} \tag{34}$$

where, $T_0 < T_1 < \cdots < T_M$ and $v_{\text{td}}(T_0) = v_{\text{td}}(T_M) = 0$, indicating that the train stops at the beginning and end of a rail interval.

Next, let $\boldsymbol{v}_{\text{gap}}$ denote the difference between the integral-based speed and time-delay-based speed at time points $\boldsymbol{t}_{\text{gap}} = \{T_0, T_1, \cdots, T_M\}$, which can be calculated by (35).

$$\begin{aligned} \boldsymbol{v}_{\text{gap}} = \{&v_{\text{td}}(T_0) - v_{\text{int}}(T_0), \ v_{\text{td}}(T_1) - v_{\text{int}}(T_1), \\ &\ldots, \ v_{\text{td}}(T_{M-1}) - v_{\text{int}}(T_{M-1}), \ v_{\text{td}}(T_M) - v_{\text{int}}(T_M)\} \end{aligned} \tag{35}$$

Let $\boldsymbol{v}_{\text{update}}$ denote the differences between the integral-based speed and time-delay-based speed at time points $\boldsymbol{t}_{\text{update}} = \{0, \Delta t, 2\Delta t, \ldots, N\Delta t\}$, which can be calculated by interpolation, as shown in (36),

$$\boldsymbol{v}_{\text{update}} = \text{interp}\left(\boldsymbol{t}_{\text{gap}}, \boldsymbol{v}_{\text{gap}}, \boldsymbol{t}_{\text{update}}\right) \tag{36}$$

where, interp$(\cdot)$ is an interpolation operator for calculating the values at $\boldsymbol{t}_{\text{update}}$, with given $\boldsymbol{t}_{\text{gap}}$ and $\boldsymbol{v}_{\text{gap}}$.

Finally, the speed estimated by data fusion, denoted as $\boldsymbol{v}_{\text{fuse}}$, can be obtained by

$$\boldsymbol{v}_{\text{fuse}} = \boldsymbol{v}_{\text{int}} + \boldsymbol{v}_{\text{update}} \tag{37}$$

IV. Application and Results

The case study was conducted on Chengdu Metro Line 7 in Chengdu, China. As mentioned in Section II, we use six smartphones to measure the 3-axis accelerations of the six cars of a metro train, respectively. The tests cover 28 stations of the metro line, so the measured data of 27 intervals can be get. Each run from the first station to the last station takes about 1.14 hours, and for comparison, we collect three runs of data.

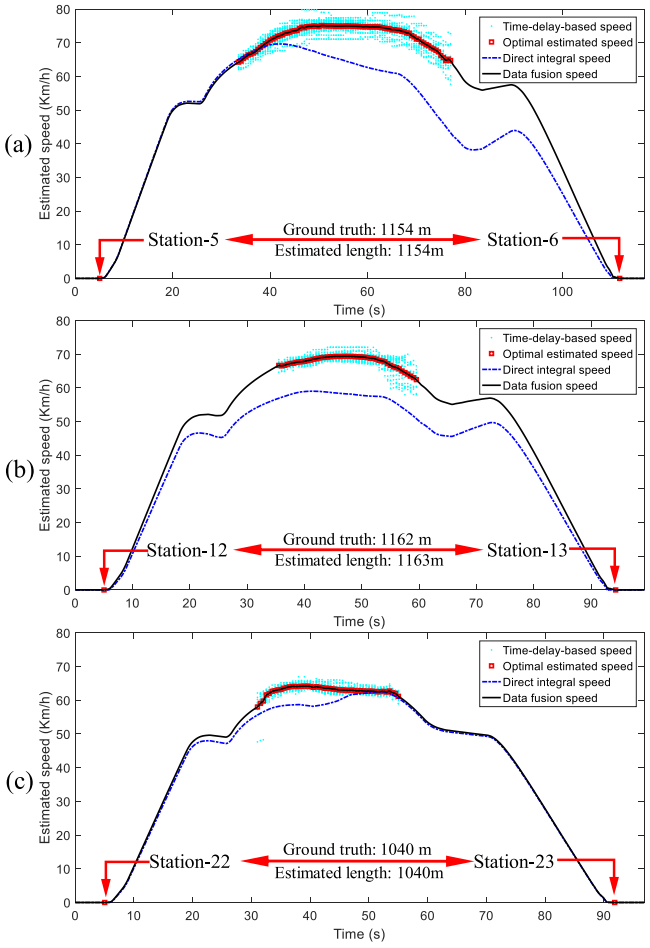

Fig. 6. Three typical cases with the time-delay-based speed (cyan), optimal estimated speed (red), direct integral speed (blue) and data fusion speed (black). (a), (b) and (c) are the results for intervals 5, 12 and 22, respectively.

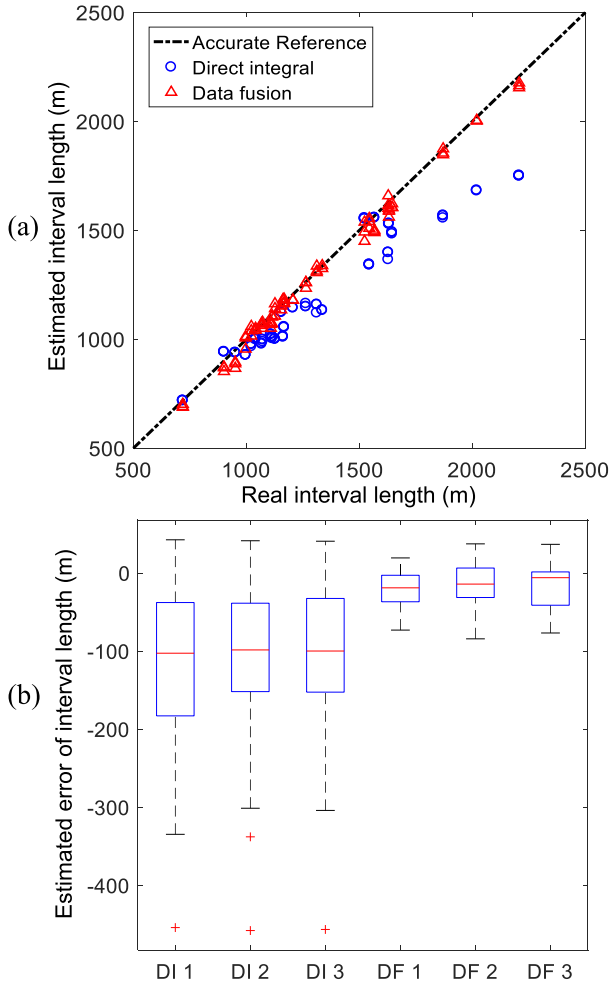

Fig. 7. The comparison between the estimated interval lengths and the ground truth. (a) shows the estimated lengths based on the direct integral method and the data fusion approach; (b) shows the distributions of the estimated errors of test runs 1,2 and 3, where DI refers to Direct Integral and DF refers to Data Fusion.

After the data preprocessing, we implement the data fusion approach and get the results of speed estimation. Fig. 6 shows three typical cases of speed-time curves, where (a), (b) and (c) are the results for intervals 5, 12 and 22, respectively. The blue dotted line represents the speed estimated by direct integral of longitudinal acceleration. The scattered cyan points are time-delay-based speed points obtained by (26). The small red boxes represent the optimal estimated speed obtained by (32). The black curve is the final data-fusion speed. It can be read from Fig. 6 that although the estimated time-delay-based speed points are scattered, they are obviously different from the integral-based speed.

The interval length between two adjacent stations is taken as the ground truth to demonstrate our data-fusion approach, since the interval length is known in advance according to the infrastructure information.

Fig. 7(a) shows the estimated interval lengths obtained by the direct integral method and the data fusion approach, with comparison to the ground truth. The black dotted line is the ground truth, namely function $f(x) = x$. The scattered points, including the blue circles and red triangles, are the estimated interval lengths. The closer the scattered points to the ground truth, the higher the accuracy of interval length estimation. The blue circles represent the estimated interval lengths obtained by double integral of the longitudinal accelerations, and the red triangles represent the estimated interval lengths obtained by the data-fusion approach. It can be found that the blue circles are farther from the ground truth for longer interval lengths, indicating that the error accumulates as the length gets longer. By contrast, the red triangles gather around the ground truth, even closer for longer interval lengths.

Fig. 7(b) illustrates the estimated errors of the interval length from statistical view using boxplots, where DI 1, 2 and 3 are the labels for the estimated errors of the direct integral method in test runs 1, 2 and 3, respectively. DF 1, 2 and 3 are the labels for the estimated errors of the data fusion approach in test runs 1, 2 and 3, respectively. It is obvious that the estimated errors of direct integral method are large, some of which even exceed 450 meters. By contrast, the estimated errors of the data-fusion approach are much smaller, most of which are less than 20 meters. Considering that the mean value of interval lengths of adjacent stations is 1310 meters, the relative error of data-fusion approach is 1.6%, while that of the direct integral method is 9.5%.

V. Discussion

This section discusses the influence of different factors on the performance of the data fusion approach. The major factors include, i) the maximal running speed of the metro train, ii) the noise of the accelerometers in smartphones, iii) the number of smartphones, iv) the interval length between two adjacent stations, v) the diversity of rail parameters.

Theoretically, for any given time T, there is a $v^*(T)$. However, the uncertainty of $v^*(T)$ relies heavily on the local waveform similarities $\rho_{i,j}$. When the train speed is relatively low, the lateral and vertical accelerations are small and easily buried in the noises. Consequently, the waveform matching between different smartphones fails, $\rho_{i,j}$ is smaller than ρ_0 and the estimated $\delta_{i,j}$ is unreliable. If most of $\delta_{i,j}$ are unreliable, there are too many zeros in the weight vector $\boldsymbol{w}$ that the final estimated $v^*(T)$ becomes meaningless. Situation becomes better when the train speed increases. The cars fully vibrate under the influence of track geometry irregularities, making waveform matching easier.

Also, the number of smartphones in use has significant influence on the performance of speed and position estimation. One or two smartphones may suffers from great uncertainties. Using more smartphones and fusing their data can effectively improve the reliability of speed and position estimation.

Furthermore, as mentioned in Section IV, for long interval lengths, the performance of the data-fusion approach is much better than the direct integral method, but for short interval lengths, the data-fusion approach doesn't show any advantages over the direct integral method. This is because for a long interval, the maximal speed of the train is higher and the rail parameters are more diverse, such as more curvatures, which makes the waveform matching more reliable, and provides more clues for speed estimation.

VI. Conclusion

In this paper, a novel data-fusion approach is proposed for speed estimation and location calibration of a metro train in underground environment, where only the data from the 3-axis accelerometers in smartphones are used. Results show that our data-fusion approach proposed reaches much higher accuracy in speed estimation than the direct integral method, because the data-fusion approach can effectively restrain the accumulated error of acceleration integral. And mostly, the total estimated error of the interval length between two adjacent stations are below 20 meters comparing to the ground truth value, even better for longer interval length. In our tests, the mean value of interval length between adjacent stations is 1310 meters, the relative error of our data-fusion approach is 1.6%, while that of the direct integral method is 9.5%, indicating that our data-fusion approach significantly improves the accuracy comparing to the direct integral method.

References

[1] H. Tang, Q. Wang, and X. Feng, "Robust stochastic control for high-speed trains with nonlinearity, parametric uncertainty, and multiple time-varying delays," *IEEE Trans. Intell. Transp. Syst.*, vol. 19, no. 4, pp. 1027–1037, Apr. 2018.

[2] M. Chou, X. Xia, and C. Kayser, "Modelling and model validation of heavy-haul trains equipped with electronically controlled pneumatic brake systems," *Control Eng. Pract.*, vol. 15, no. 4, pp. 501–509, 2007.

[3] X. Zhuan and X. Xia, "Optimal scheduling and control of heavy haul trains equipped with electronically controlled pneumatic braking systems," *IEEE Trans. Control Syst. Technol.*, vol. 15, no. 6, pp. 1159–1166, Nov. 2007.

[4] J. Otegui, A. Bahillo, I. Lopetegi, and L. E. Díez, "A survey of train positioning solutions," *IEEE Sensors J.*, vol. 17, no. 20, pp. 6788–6797, Oct. 2017.

[5] Q. Zhang, X. Niu, H. Zhang, and C. Shi, "Algorithm improvement of the low-end GNSS/INS systems for land vehicles navigation," *Math. Problems Eng.*, vol. 2013, pp. 1–12, Jun. 2013.

[6] S. Bedrich and X. Gu, "GNSS-based sensor fusion for safety-critical applications in rail traffic," in *Proc. Galileo EGNOS Inf. Catalogue*, 2004, p. 8.

[7] T. Albrecht, K. Lüddecke, and J. Zimmermann, "A precise and reliable train positioning system and its use for automation of train operation," in *Proc. IEEE Int. Conf. Intell. Rail Transp.*, Beijing, China, Aug./Sep. 2013, pp. 134–139.

[8] P. Salvatori, A. Neri, C. Stallo, V. Palma, A. Coluccia, and F. Rispoli, "Augmentation and integrity monitoring network and EGNOS performance comparison for train positioning," in *Proc. 22nd Eur. Singal Process. Conf. (EUSIPCO)*, Lisbon, Portugal, Sep. 2014, pp. 186–190.

[9] J. Liu, T. Tang, B. Gai, J. Wang, and D. Chen. "Integrity assurance of GNSS-based train integrated positioning system," *Sci. China Technol. Sci.*, vol. 54, no. 7, pp. 1779–1792, 2001.

[10] B. Cai and X. Wang, "Train positioning via integration and fusion of GPS and inertial sensors," *WIT Trans. Built Environ.*, vol. 50, pp. 1217–1226, Aug. 2000.

[11] E. J. Barlow, "Doppler radar," *Proc. IRE*, vol. 37, no. 4, pp. 340–355, Apr. 1949.

[12] S. Gezici *et al.*, "Localization via ultra-wideband radios: A look at positioning aspects for future sensor networks," *IEEE Signal Process. Mag.*, vol. 22, no. 4, pp. 70–84, Jul. 2005.

[13] M. Malvezzi, G. Vettori, B. Allotta, L. Pugi, A. Ridolfi, and A. Rindi, "A localization algorithm for railway vehicles based on sensor fusion between tachometers and inertial measurement units," *Proc. School Mech. Eng. F, J. Rail Rapid Transit*, vol. 228, no. 4, pp. 431–448, 2014.

[14] B. Allotta, V. Colla, and M. Malvezzi, "Train position and speed estimation using wheel velocity measurements," *Proc. School Mech. Eng. F, J. Rail Rapid Transit*, vol. 216, no. 3, pp. 207–225, 2002.

[15] A. Mirabadi, N. Mort, and F. Schmid, "Application of sensor fusion to railway systems," in *Proc. IEEE/SICE/RSJ Int. Conf. Multisensor Fusion Integr. Intell. Syst.*, Washington, DC, USA, Dec. 1996, pp. 185–192.

[16] A. R. Jiménez, F. Seco, J. C. Prieto, and J. Guevara, "Indoor pedestrian navigation using an INS/EKF framework for yaw drift reduction and a foot-mounted IMU," in *Proc. 7th Workshop Positioning, Navigat. Commun.*, Dresden, Germany, Mar. 2010, pp. 135–143.

[17] K. Kim, S.-H. Kong, and S.-Y. Jeon, "Slip and slide detection and adaptive information sharing algorithms for high-speed train navigation systems," *IEEE Trans. Intell. Transp. Syst.*, vol. 16, no. 6, pp. 3193–3203, Dec. 2015.

[18] G. Lombaert, G. Degrande, S. François, and D. J. Thompson, "Ground-borne vibration due to railway traffic: A review of excitation mechanisms, prediction methods and mitigation measures," in *Noise and Vibration Mitigation for Rail Transportation Systems* (Notes on Numerical Fluid Mechanics and Multidisciplinary Design), vol. 126. Berlin, Germany: Springer, 2015, pp. 253–287.

[19] M. J. Griffin, "Discomfort from feeling vehicle vibration," *Vehicle Syst. Dyn.*, vol. 45, nos. 7–8, pp. 679–698, 2007.

[20] O. Thuong and M. J. Griffin, "The vibration discomfort of standing persons: 0.5–16-Hz fore-and-aft, lateral, and vertical vibration," *J. Sound Vib.*, vol. 330, no. 4, pp. 816–826, Feb. 2011.

[21] O. Thuong and M. J. Griffin, "The vibration discomfort of standing people: Evaluation of multi-axis vibration," *Ergonomics*, vol. 58, no. 10, pp. 1647–1659, 2015.

[22] A. M. Kaynia, J. Park, and K. Norén-Cosgriff, "Effect of track defects on vibration from high speed train," *Procedia Eng.*, vol. 199, pp. 2681–2686, Jan. 2017.

[23] S. Kaewunruen, M. Ishida, and S. Marich, "Dynamic wheel–rail interaction over rail squat defects," *Acoust. Aust.*, vol. 43, no. 1, pp. 97–107, 2015.

[24] Z. Liu, F. Li, B. Huang, and G. Zhang, "Real-time and accurate rail wear measurement method and experimental analysis," *J. Opt. Soc. Amer. A, Opt. Image Sci.*, vol. 31, no. 8, pp. 1721–1729, 2014.

[25] A. Coulon, B. Nélain, and N. Vincent, "Interest of equivalent damage methods for railway equipment qualification to vibrations," *Procedia Eng.*, vol. 133, pp. 714–725, Jan. 2015.
[26] Z. Wang, Y. Yu, L. Zhang, Y. Li, and W. Yang, "Health status evaluation approach of critical equipment in an urban rail transit system," in *Proc. 5th Int. Conf. Transp. Eng.*, Dalian, China, Sep. 2015, pp. 2196–2208.
[27] H. Tsunashima, Y. Naganuma, and T. Kobayashi, "Track geometry estimation from car-body vibration," *Vehicle Syst. Dyn.*, vol. 52, pp. 207–219, Mar. 2014.
[28] E. Denti, R. Galatolo, and F. Schettini, "An AHRS based on a Kalman filter for the integration of inertial, magnetometric and GPS data," in *Proc. 27th Int. Congr. Aeronaut. Sci.*, 2010, pp. 1–9.
[29] K. R. Anne, K. Kyamakya, F. Erbas, C. Takenga, and J. C. Chedjou, "GSM RSSI-based positioning using extended Kalman filter for training artificial neural networks," in *Proc. 60th IEEE Veh. Technol. Conf.*, Los Angeles, CA, USA, Sep. 2004, pp. 4141–4145.
[30] I. Arasaratnam and S. Haykin, "Cubature Kalman filters," *IEEE Trans. Autom. Control*, vol. 54, no. 6, pp. 1254–1269, Jun. 2009.
[31] J. Liu, B.-G. Cai, T. Tang, and J. Wang, "A CKF based GNSS/INS train integrated positioning method," in *Proc. IEEE Int. Conf. Mechatronics Autom.*, Xi'an, China, Aug. 2010, pp. 1686–1689.
[32] J. Liu, B.-G. Cai, and J. Wang, "Track-constrained GNSS/odometer-based train localization using a particle filter," in *Proc. IEEE Intell. Vehicles Symp. (IV)*, Gothenburg, Sweden, Jun. 2016, pp. 877–882.
[33] Z. Chen, "Bayesian filtering: From Kalman filters to particle filters, and beyond," *Statistics*, vol. 182, no. 1, pp. 1–69, 2003.
[34] S. S. Saab, "A map matching approach for train positioning Part I: Development and analysis," *IEEE Trans. Veh. Technol.*, vol. 49, no. 2, pp. 467–475, Mar. 2000.
[35] S. S. Saab, "A map matching approach for train positioning Part II: Application and experimentation," *IEEE Trans. Veh. Technol.*, vol. 49, no. 2, pp. 476–484, Mar. 2000.
[36] K. Gerlach and M. M. Z. Hörste, "A precise digital map for GALILEO-based train positioning systems," in *Proc. 9th Int. Conf. Intell. Transp. Syst. Telecommun.*, Lille, France, Oct. 2009, pp. 343–347.
[37] K. Lüddecke and C. Rahmig, "Evaluating multiple GNSS data in a multi-hypothesis based map-matching algorithm for train positioning," in *Proc. IEEE Intell. Vehicles Symp. (IV)*, Baden-Baden, Germany, Jun. 2011, pp. 1037–1042.
[38] K. Gerlach and C. Rahmig, "Multi-hypothesis based map-matching algorithm for precise train positioning," in *Proc. 12th Int. Conf. Inf. Fusion*, Seattle, WA, USA, Jul. 2009, pp. 1363–1369.
[39] M. Ilyas, K. Cho, S.-H. Baeg, and S. Park, "Drift reduction in IMU-only pedestrian navigation system in unstructured environment," in *Proc. 10th Asian Control Conf.*, Kota Kinabalu, Malaysia, May/Jun. 2015, pp. 1–7.
[40] Y. Wang, P. Wang, X. Wang, and X. Liu, "Position synchronization for track geometry inspection data via big-data fusion and incremental learning," *Transp. Res. C, Emerg. Technol.*, vol. 93, pp. 544–565, Aug. 2018.

Yuan Wang received the B.S. degree in civil engineering from Southwest Jiaotong University, Chengdu, China, in 2014, where he is currently pursuing the Ph.D. degree with the School of Civil Engineering. He is also a visiting Ph.D. student with the Department of Civil and Environmental Engineering, Rutgers, The State University of New Jersey, New Jersey, USA.

His current research focuses on rail measurement techniques, big data application of track maintenance, intelligent railway system, and nonlinear dynamics. He is also fond of APP designing for Android and IOS.

Jianli Cong was born in Suzhou, Anhui. He received the B.S. degree in highway and railway engineering from Lanzhou Jiaotong University, Lanzhou, China. He is currently pursuing the master's degree with the School of Civil Engineering, Southwest Jiaotong University.

His research interest includes track condition monitoring.

Ping Wang received the Ph.D. degree in highway and railway engineering from Southwest Jiaotong University, Chengdu, China.

He designed and developed high-speed track turnout with a speed of 350 km/h in China and resolved the technical challenge of laying track turnout over bridge. He is currently a Professor with the School of Civil Engineering, Southwest Jiaotong University, and the Head of the Key Laboratory of High-Speed Railway Engineering, Ministry of Education, China. He has authored a book *Design and Practice of High-Speed Track Turnout*. His research interests include the theory and dynamics of high-speed track turnout and the track structure of high-speed railway.

Xiang Liu received the B.S. degree in transportation engineering from Shanghai Jiaotong University, Shanghai, China, in 2008, and the M.S. and Ph.D. degrees in civil engineering from the University of Illinois at Urbana–Champaign (UIUC), Champaign, IL, USA, in 2011 and 2013, respectively.

He is currently an Assistant Professor with the Department of Civil and Environmental Engineering, Rutgers, The State University of New Jersey, New Jersey, USA. He has published over 100 papers in peer-reviewed journals and international conferences. His research interests are focus on, artificial intelligence (AI), big data, and automation technologies for improving rail operational safety and efficiency.

Prof. Liu has received four Best Paper Awards from the Transportation Research Board (TRB), the Educator of the Year 2017 Award, and the Researcher of the Year 2018, both in New Jersey. In 2018, he was recognized by a Rising Star Award from the Progressive Railroading Magazine.

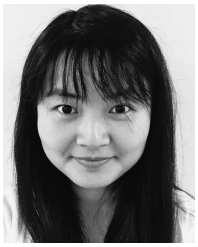

Huiyue Tang received the B.S. degree in electrical engineering and automation from Southwest Jiaotong University, Chengdu, China in 2014, where she is currently pursuing the Ph.D. degree with the School of Electrical Engineering. She is also a visiting Ph.D. student with the Department of Civil and Environmental Engineering, Rutgers, The State University of New Jersey, New Jersey, USA.

Her research interests lie in automatic train control, reinforcement-learning-based optimization and control techniques, robust and adaptive control, and data-fusion-based rail measurement techniques.